Materialia 15 (2021) 101023

Contents lists available at ScienceDirect

Materialia

journal homepage: www.elsevier.com/locate/mtla

Full Length Article

Effects of recoil spectra and electronic energy dissipation on defect survival in 3C-SiC

Lauren Nuckols[a,*], Miguel L. Crespillo[a], Yang Yang[b], Ju Li[c], Eva Zarkadoula[d], Yanwen Zhang[d], William J. Weber[a,*]

[a] Materials Science and Engineering, University of Tennessee, Knoxville, TN 37996, USA
[b] National Center for Electron Microscopy (NCEM), Molecular Foundry, Lawrence Berkeley National Laboratory, Berkeley CA 97720, USA
[c] Department of Nuclear Science and Engineering and Department of Materials Science and Engineering, MIT, Cambridge, MA 02139, USA
[d] Materials Science and Technology Division, Oak Ridge National Laboratory, Oak Ridge, TN 37831, USA

ARTICLE INFO

Keywords:
Silicon carbide
Ion irradiation
Irradiation effect
Defects
Ionization

ABSTRACT

The coincidence of electronic and damage energy dissipation from energetic ions to an atomic lattice can significantly affect damage production along the ion trajectory due to spatial overlap of inelastic and elastic processes. Damage production and disordering in single crystal 3C-SiC from 5 MeV Si and 10 MeV Au ions is investigated using ion-channeling experiments. While defects are created by damage energy dissipation via elastic scattering, electronic energy dissipation via electron-phonon coupling decreases defect survival along the ion trajectory for Si ions. The more energetic recoil spectrum for 10 MeV Au ions leads to weaker spatial coupling of electronic and damage energy dissipation processes, and damage production is only weakly affected.

Introduction

Silicon carbide (SiC) is a wide bandgap semiconductor [1] that is mechanically and chemically inert at elevated temperatures [2,3] and has a small neutron absorption cross-section [4,5], and because of these properties, SiC and SiC-based composites are candidate structural and electronic materials for harsh environments, particularly nuclear and space applications. Sintered SiC has been used as a light weight mirror material for space applications [6] and single crystal SiC wafers have been used for various electronic devices for space exploration [7–10]. In these space applications, material degradation and single-event upsets due to cosmic radiation are a concern. The cubic 3C-SiC polytype is especially useful as a nuclear material as it, in polycrystalline form, is used as a cladding layer in TRISO (tristructural-isotropic) fuel particles [4] and as both the fibers and matrix in SiC_f/SiC_m composites [11], which are potential structural materials for accident tolerant cladding, Gen IV advanced reactors, and fusion reactors [11–14].

As a nuclear material, understanding irradiation effects in SiC is necessary to develop predictive models for performance lifetimes of reactor structural components and in-reactor sensors. Often ions are used to simulate neutron irradiation, as ion irradiation from accelerators can produce far greater doses and higher dose rates than fission test reactors, which are limited to damage rates below 20 dpa/year [15]. Electronic excitations, i.e., ionization effects, can be much more prevalent under high-energy ion irradiations compared to fast neutron irradiations as ions are charged, and the proportion of kinetic energy lost to electronic excitation increases with ion velocity [16,17]. However, fast neutrons produce damage by transferring kinetic energy to atoms in a material, thereby creating charged recoil atoms (i.e., ions), which are generally referred to as primary knock-on atoms (PKAs), and these PKAs have higher average energy than recoils produced along an ion trajectory [16,18]. Thus a larger fraction of PKA energy is lost to electronic excitation compared to recoils created via ion irradiation. Ceramic materials are particularly sensitive to ionization effects, as they can lead to: 1) amorphization along the ion path [19–21]; 2) additive damage production from combined electronic and damage energy dissipation [22,23]; 3) synergistic damage production from electronic energy interactions with pre-existing defects [24,25]; 4) annealing of pre-existing defects [26,27], and 5) decreased survival of in-cascade defects [28,29]. In SiC, electronic energy dissipation leads to annealing of defect structures, which can be important in device fabrication, as well as in both space and nuclear applications. This ionization-induced annealing process competes with damage energy dissipation by elastic scattering, and under some conditions can totally suppress or limit damage accumulation [27–30]. Electronic energy dissipation effects are present in SiC under neutron irradiations, as fission and fusion neutrons produce energetic PKAs up to several hundred keV and several MeV, respectively; these PKAs lose most of their energy to electrons via ionization. As a

* Corresponding authors.
E-mail addresses: lnuckols@vols.utk.edu (L. Nuckols), wjweber@utk.edu (W.J. Weber).

https://doi.org/10.1016/j.mtla.2021.101023
Received 13 January 2021; Accepted 24 January 2021
Available online 28 January 2021

result, the overall effects of ionization can be significant, and must be considered when developing predictive performance models based on using ion irradiation as a surrogate for neutron irradiation of SiC, as ionization-induced processes can affect both damage production and accumulation processes. In addition, ionization effects are critically important in SiC-based devices in space applications.

The electronic stopping power for an ion is defined as the energy loss to electrons per unit pathlength; however, since incident ions generally do not follow a straight path normal to the surface, the electronic energy loss (i.e., ionization energy deposition) by an incident ion at some depth is generally taken as the average energy transferred inelastically to electrons per unit depth, which is readily calculated using several available Monte Carlo simulation codes, such as SRIM [31], Iradina [32], or IM3D [33,34]. Likewise, the total ionization energy deposited per unit depth by the passage of an incident ion is the sum of the average energy loss to electrons at some depth by both the incident ion and all the primary and secondary atomic recoils, which can also be calculated by the same simulation codes. Previous work at room temperature found that ionization-induced recovery of pre-existing defects has an electronic energy loss threshold value of 1.4 keV/nm for this athermal annealing process to occur [27]. This threshold of 1.4 keV/nm is a relatively low value of electronic energy loss, as most low to intermediate energy ions employed in research, as well as cosmic radiation have much greater electronic energy loss values. Furthermore, this threshold for ionization-induced annealing processes, in terms of equivalent PKA energies, is 750 keV for Si and 850 keV for C PKAs, well below the typical PKA energies produced by fusion neutrons, but only a small fraction of fission-neutron PKAs exceed such energies. For in-cascade processes in SiC, where damage energy dissipation (energy that goes into producing displaced atoms and dissipated via phonons) is temporally and spatially coupled with the total ionization energy dissipation, the threshold in electronic energy loss to induce measurable in-cascade annealing was found to be 1.0 keV/nm in a study of 3C-SiC irradiated with 1.5 and 5.0 MeV Si ions [28]. This threshold value corresponds to PKA energies of about 450 keV for both Si and C PKAs.

Coupled defect production and annealing along ion trajectories depends on both the respective magnitudes of the electronic and damage energy dissipation, as well as the ratios between the dissipation processes [30], which is best described as the ratio of total ionization energy to damage energy. The dissipation of ionization energy for an incident ion is often modeled as a radially localized thermal spike along the ion path lasting tens of ps to several hundred ps [35]. In general, the thermal spike intensity increases with increasing electronic energy loss. Irradiation damage in SiC is the accumulation of defects produced by ballistic collisional processes (i.e., damage energy dissipation) that survive or extend radially beyond the ionization-induced thermal spike [30]. Greater elastic energy dissipation results in more energetic atomic recoils and defect production beyond the extent of the thermal spike. Additionally, because the ionization-induced thermal spikes are transient, short-lived events, the coupled annealing processes may be most effective for point defects, leaving defect clusters mostly intact.

In this study, the effects of recoil spectra and ratio of total ionization energy to damage energy dissipation are investigated in 3C-SiC single crystals by comparing defect survival from 10 MeV Au ions with previous results for self-ion irradiation using 5 MeV Si ions. The 10 MeV Au and 5 MeV Si ions have comparable pathlengths and electronic energy loss values. However, while self-ion irradiations are generally recommended [16], nuclear energy loss and damage energy for the 5 MeV Si ions are significantly lower than for 10 MeV Au ions. By comparing measured rates of disorder accumulation at different depths, the effects of recoil spectra and total ionization to damage energy ratio can be evaluated based on predicted recoil spectra and radial dissipation of ionization and damage energy. The results reveal that coupling between ionization and damage energy dissipation for the Si ions is stronger, and therefore defect survival along the ion trajectory is more sensitive to changes in ionization energy. In contrast, the more energetic recoil spectra resulting from the 10 MeV Au ions leads to weaker spatial coupling of inelastic and elastic process, which results in more damage survival at similar doses, as well as significantly reduced (by a factor of 20 or more) implanted ion concentrations, compared to 5 MeV Si irradiations.

Experimental methods

In this study, single crystal, 3C-SiC thin films in (001) orientation on a silicon substrate were grown by NOVA Electronic Materials. The 3C-SiC film layer thickness is 3.8 μm, therefore any strain from film-substrate lattice mismatch is undetectable, as the maximum depth region of interest is only 1.5 μm from the surface. The 3 MV tandem accelerator and associated facilities at the Ion Beam Materials Laboratory (IBML) [36] were used to perform the ion irradiations and characterize disorder via Rutherford backscattering spectrometry in channeling geometry (RBS/C). The 5 MeV Si ions and 10 MeV Au ions were chosen because of similar electronic stopping powers and ion depth ranges, but significant differences in nuclear stopping powers and thus damage energy dissipation along the ion trajectories. For both ions, the irradiations were performed at 60° off the (001) surface normal to create shallow damage that provided for more accurate analysis of disorder profiles by RBS/C. Ion fluences ranged from 8.7×10^{13} to 1.9×10^{15} ions/cm^2 for the 5 MeV Si ions and from 5.0×10^{12} to 1.0×10^{14} ions/cm^2 for the 10 MeV Au ions. Ion fluxes were 1.4×10^{12} ions/cm^{2}s for the 5 MeV Si irradiations and 1.9×10^{11} ions/cm^{2}s for the Au irradiations. The maximum temperature increase due to beam heating was estimated based on power density calculations and was determined to be less than 8 K for both irradiation conditions. The RBS/C measurements were performed in situ along the [001] direction using 3.5 MeV He ions. The irradiations and RBS/C characterization were performed at 300 K under vacuum below 2.0×10^{-7} Torr.

The depth profiles of atomic displacements and energy deposition for the 5 MeV Si ions at an incident angle of 60° were determined using the SRIM 2010 code [31] in full-cascade mode, as recently recommended [37]. Because the electronic stopping powers for Au ions in SiC are overestimated by the SRIM code [38], the depth profiles of displacements and energy deposition for the 10 MeV Au ions at an incident angle of 60° were determined using the IM3D code [33] in full-cascade mode, which utilized new experimentally derived electronic stopping powers for Au ions in SiC that correctly predict the Au implantation profiles for energies up to 15 MeV [37,38], as illustrated in Fig.S1 for 10 MeV Au ions implanted at 60°. For both the SRIM and IM3D full-cascade simulations, threshold displacement energies of 35 eV for Si and 20 eV for C [39] and lattice binding energies of 0 eV were used. A density of 3.21 g/cm^3 was assumed. The predicted displacement damage profiles for the irradiation conditions of this study are shown in Fig. 1. In the case of the 10 MeV Au ions, the results of full-cascade SRIM simulations are included in Fig. 1b for comparison, which clearly indicate the increase in number of displacements to deeper depths from the IM3D simulations due to the lower electronic energy stopping powers employed for Au ions in SiC. Results of IM3D calculations for 5 MeV Si ions are also included in Fig. 1a to show the good agreement between SRIM and IM3D calculations for the same SRIM predicted electronic stopping powers. The main difference in the two codes is how the scattering cross sections are implemented, as described elsewhere [34]. In this study, the SRIM results for 5 MeV Si ions and the IM3D results for 10 MeV Au ions are used to calculate the damage dose (displacements per atom or dpa) at different depths for each ion fluence, as well as the depth profiles of energy dissipation.

Because of the significant effects of ionization-induced annealing in SiC [27,28,30,40], the amount of energy loss to electrons by the incident ion and recoils (i.e., total ionization energy) along the incident ion trajectory relative to the damage energy, which is the elastic energy that goes into creating displacements, is an important consideration in the evaluation of experimental results. The depth profiles of total ionization energy and damage energy deposition, as measured in units of

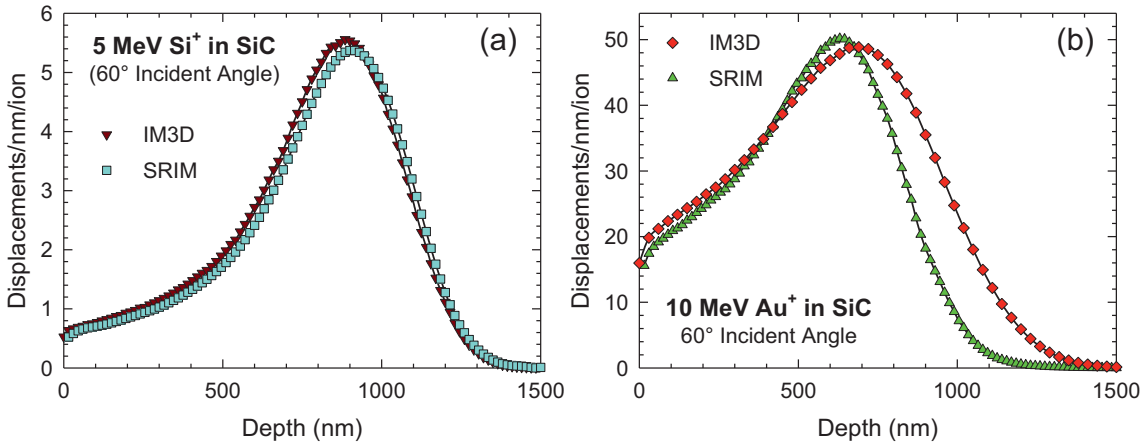

Fig. 1. Depth profiles of displacement production (damage) per ion: (a) 5 MeV Si ions incident at an angle of 60°, based on full-cascade SRIM and IM3D simulations; (b) 10 MeV Au ions incident at an angle of 60°, based on full-cascade IM3D simulation that employ a new experimentally-derived electronic stopping power for Au ions in SiC [33], and full-cascade SRIM simulations that utilize the SRIM predicted electronic stopping power.

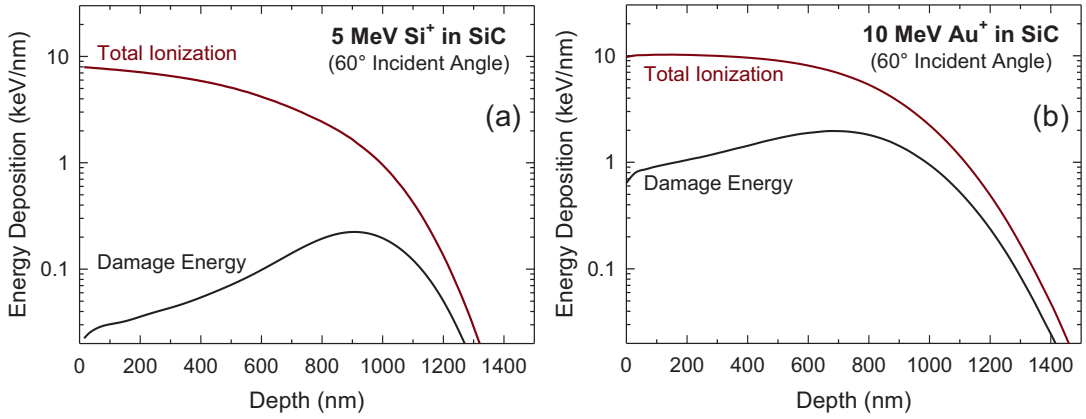

Fig. 2. The partitioning of incident ion energy (per unit depth) to total ionization energy (inelastic energy transfer to electrons by the incident ion and secondary recoils) and to the damage energy (elastic energy going into atomic displacements): (a) 5 MeV Si ions in SiC at an incident angle of 60°; and (b) 10 MeV Au ions at an incident angle of 60°.

keV per unit incremental depth (not pathlength), are shown in Fig. 2, where the damage energy profiles were determined from the total energy dissipated to phonons, as described previously [37,41]. While the total ionization energy for both 5 MeV Si and 10 MeV Au ions is much larger than the damage energy, the damage energy for the 5 MeV Si ions (Fig. 2a) is significantly less than the damage energy for the 10 MeV Au ions (Fig. 2b). The ratio of total ionization energy to damage energy is one indicator of the effect of spatial and temporal coupling of inelastic and elastic energy loss processes on defect survival and damage accumulation

A major effect of the lower damage energy for the 5 MeV Si ions shown in Fig. 2(a) is a softer primary recoil energy spectrum compared to 10 MeV Au ions. The primary recoil spectra for 5 MeV Si and 10 MeV Au ions were determined by using pysrim [42] to examine the full-cascade collision files created by the SRIM 2008 code for 10,000 incident ions of each type. The primary recoil spectrum for 10 MeV Au ions depends on the scattering cross sections and not the electronic stopping power, so the SRIM 2008 calculations are valid for this determination. While the primary recoil spectrum for a given ion is important, a more meaningful measure of the overall effect of recoil spectrum on defect production is the weighted primary recoil spectrum, W(T), which is the fraction of displaced atoms produced by all primary recoils with energies less than a given primary recoil energy [43]. The weighted recoil spectra for 5 MeV Si and 10 MeV Au ions in SiC are shown in Fig. 3, along with the weighted recoil spectra in SiC for neutrons in the High

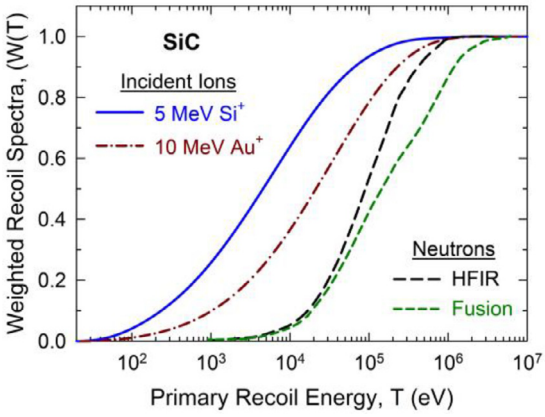

Fig. 3. Weighed primary recoil spectra for 5 MeV Si and 10 MeV Au ions in SiC, along with that for neutron irradiations in HFIR and a fusion reactor [44].

Flux Isotope Reactor (HFIR) and a fusion reactor [44]. Based on the same 10,000 full-cascade collision files from SRIM, the pysrim code was used to determine the radial distributions of damage energy deposition and defect production along the incident ion trajectory for both 5 MeV Si and 10 MeV Au ions, as described previously for other incident ions in SiC

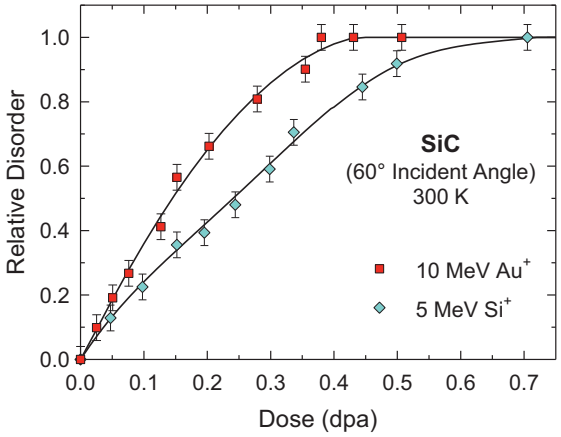

Fig. 4. Relative disorder on Si sublattice at the damage peak as a function of damage dose in 3C-SiC irradiated with 5 MeV Si ions and 10 MeV Au ions.

[30]. These radial distributions will be compared to ionization energy deposition via electron-phonon coupling in the discussion section.

Results

The RBS/C results on the depth profiles of relative Si-lattice disorder as a function of 5 MeV Si ion fluence have been previously reported [28], and the RBS/C spectra and disorder depth profiles as a function of ion fluence for the 10 MeV Au irradiation are provided in Fig. S2 in the Supplementary Material. From the RBS/C data, the accumulation of relative disorder at the depth corresponding to the damage peak has been determined as a function of damage dose (dpa) for both the 5 MeV Si and 10 MeV Au irradiation, and the results are compared in Fig. 4. The Au ion irradiations are much more efficient than Si ions in disordering SiC, and a fully amorphous state is achieved at a dose of about 0.4 dpa under 10 MeV Au ion irradiation. For the 5 MeV Si ions, full amorphization requires a dose of about 0.7 dpa. Similar differences in disorder accumulation behavior at the damage peak has been previously reported in 6H-SiC irradiated at 170 to 190 K by 0.55 MeV Si ions and 2.0 MeV Au ions [45]. At 150 K, the disorder accumulation behavior is nearly identical [46] for the same Si and Au ions, indicating that damage accumulation behavior under Si ion irradiation is more sensitive to athermal or thermal annealing behavior. The dose for full amorphization at the damage peak in 3C-SiC under 10 MeV Au ion irradiation (current study) is nearly the same as that for 6H-SiC under 2 MeV Au ion irradiation at 300 K [47], suggesting that the high density of ionization energy from 10 MeV Au ions at the damage peak may have a minimal effect on defect survival at the damage peak. Similarly, the damage accumulation behavior at the damage peak for the 5 MeV Si ions is identical to that under 1.5 MeV Si ions at 300 K, as reported previously [28]; however, ionization-induced recovery processes were more pronounced for 5 MeV Si ions than 1.5 MeV Si ions at shallow depths (200 to 500 nm). The current and previous results indicate that the harder primary recoil spectrum (Fig. 3) and higher damage energy per ion (Fig. 2a) for Au ions produce more stable defects and greater in-cascade defect survivability than the Si ions, which is consistent with molecular dynamics simulations of relative defect size distributions [48]. Further, the high values of the total ionization energy deposited per ion (Fig. 2) relative to the damage energy deposited can enhance annealing of surviving defects along the ion trajectories, as discussed in more detail below.

Based on the disorder depth profiles versus fluence data, the dependencies of relative disorder on local damage dose (dpa) at shallower depths have been determined and are presented in Fig. 5. While the ionization energies are of comparable magnitude over the first several hundred nanometers of depth (Fig. 2), the decrease in rate of disordering is more pronounced near the surface (200 to 400 nm) under 5 MeV Si ion irradiation (Fig. 5a) than under 10 MeV Au ion irradiation (Fig. 5b). The most significant effect of the total ionization energy is near the surface, where the total ionization energy deposition is maximized and the damage energy is minimized for both 5 MeV Si and 10 MeV Au ions. The effect diminishes with increasing depth as the energy of the incident ions decreases. However, the total ionization energy deposition is dominant over the damage energy deposition over the entire depth of damage for both 5 MeV Si and 10 MeV Au ions. The total ionization energy, damage energy, and ratio of ionization energy to damage energy at each depth are summarized in Table 1.

Temporal and spatial coupling of inelastic ionization energy dissipation and elastic damage energy dissipation to the atomic structure are critical to understanding primary defect production and damage evolution. Evidence for ionization-induced annealing along energetic ion tracks, as well as ionization-induced in-cascade annealing, have been previously reported [28,30,49,50]. At 300 K, where thermal annealing processes in SiC are small compared to ionization-induced annealing, these studies demonstrated that the inverse dose for amorphization, $1/D$, is linearly dependent on the ratio of the ionization-induced recovery cross section, σ_i, to the elastic damage cross section, σ_d, and is given by the general expression:

$$1/D = (1/D_o)\left[1 - (\sigma_i/\sigma_d)\exp(-E_{irr}/kT)\right], \quad (1)$$

where D_o is the amorphization dose at 0 K or at a temperature where flux effects are negligible and E_{irr} is the activation energy for the ionization-induced recovery. Eq. (1) can be applied to the dose to achieve an amor-

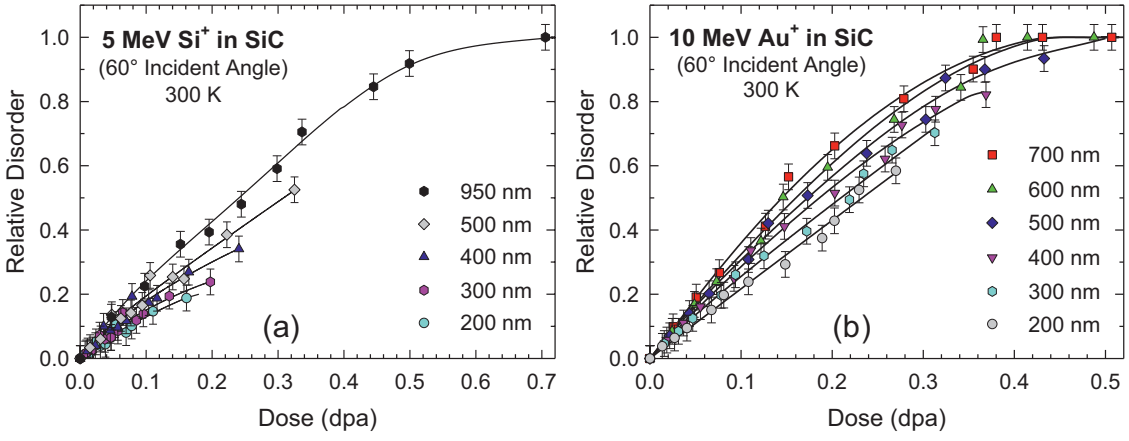

Fig. 5. Relative disorder fraction on the Si sublattice in 3C-SiC as a function of damage dose (dpa) at different depths: (a) 5 MeV Si ions in SiC at an incident angle of 60° (adapted from Ref. [28]); and (b) 10 MeV Au ions at an incident angle of 60°.

Table 1
SRIM (5 MeV Si) and IM3D (10 MeV Au) predicted total ionization energy and damage energy deposition at different depths, along with the ratio of total ionization to damage energy.

Depth (nm)	5 MeV Si at 60° Ionization Energy (keV/nm)	Damage Energy (keV/nm)	Ratio	10 MeV Au at 60° Ionization Energy (keV/nm)	Damage Energy (keV/nm)	Ratio
200	7.1	0.04	177.5	10.2	1.05	9.7
300	6.6	0.04	165.0	10.0	1.22	8.2
400	5.9	0.05	118.0	9.6	1.42	6.8
500	5.1	0.07	72.9	9.0	1.70	5.3
600	4.2	0.10	42.0	8.1	1.89	4.3
700	3.2	0.14	22.9	6.9	1.96	3.5
800	2.4	0.19	12.6	5.3	1.82	2.9
900	1.7	0.22	7.7	3.7	1.43	2.6

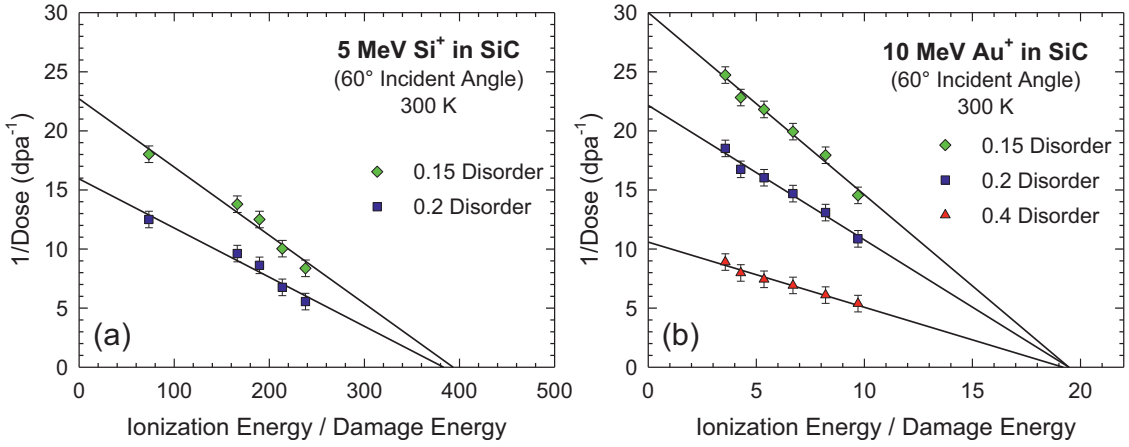

Fig. 6. Linear dependence of inverse dose to achieve a specific level of disorder on ratio of ionization energy to damage energy in SiC at 300 K: (a) disorder levels of 0.15 and 0.20 under 5 MeV Si irradiation; and (b) disorder levels of 0.15, 0.20 and 0.40 under 10 MeV Au irradiation.

phous state or a specific level of disorder in SiC. At constant temperature (300 K), the *exp* term is just a constant, *C*, and the inverse dose to achieve a specific disorder level is proportional to σ_i/σ_d with a slope C/D_o. The ratio σ_i/σ_d is directly proportional to the ratio of total ionization energy to damage energy at a given depth, which can be determined from the data in Fig. 2 and is summarized in Table 1. The doses to achieve disorder levels of 0.15 and 0.2 under 5 MeV Si irradiation and disorder levels of 0.15, 0.2, and 0.4 under 10 MeV Au irradiation are determined from curve fits in Fig. 5, and the inverse doses to achieve these specific levels of disorder are linearly dependent on the ratio of total ionization energy to damage energy, as shown in Fig. 6. The results indicate that a unique dose to achieve similar levels of disorder at 0 K (*y*-axis intercept) is larger for the 5 MeV Si ions than for the 10 MeV Au ions for an equivalent level of damage (e.g., 0.15 and 0.2 disorder). In the case of Si ions, the results in Fig. 6a suggest that, above an ionization energy to damage energy ratio of 390, it may not be possible to achieve disorder levels above 0.15 to 0.2, which could suggest saturation levels of disorder with ionization-induced annealing processes in equilibrium with damage production from elastic collision processes. A slightly higher ionization energy to damage energy ratio may be required to suppress a disorder level above 0.15 compared to 0.2 under 5 MeV Si ion irradiation, which is not unexpected. In the case of Au ions (Fig. 6b), there is not much difference in the ionization energy to damage energy ratio to suppress disorder levels between 0.15 and 0.4, and a ratio of 20 may suppress achieving disorder levels above 0.5. These results are consistent with the observed full suppression of damage accumulation in 4H-SiC under 21 MeV Si ion irradiation (total ionization energy to damage energy ratio exceeding 940) and the predicted full suppression of all damage accumulation at a total ionization energy to damage energy ratio of 33 in 6H-SiC irradiated with 25 MeV Au ion at 300 K [30].

Discussion

In order to better understand the coupling of ionization energy and damage energy along the actual trajectory or pathlength of an ion, the radial dissipation of both the ionization energy and the damage energy to the atomic structure are examined. The radial dissipation of damage energy along the ion pathlength for incident ions cannot be estimated directly from the SRIM full-cascade collision files. To determine this, the radial distributions of displacements for 5 MeV Si and 10 MeV Au are first ascertained using pysrim [42] to examine 10,000 full-cascade collision files created by the SRIM 2008 code for each ion type over the pathlength segment from 700 to 800 nm (corresponding to a depth from 350 to 400 nm for an incident angle of 60°). These radial distributions of displacements are illustrated in Fig. 7a and 7b, and the significant greater radial extent of displacements from 10 MeV Au ions is due to the harder primary recoil spectrum for Au ions compared to Si ions over this depth range (Fig. 3). Using the total integrated number of displacements (Fig. 1) and the integrated damage energy (Fig. 2) from full cascade simulations for each ion, the average amount of damage energy deposited per displacement event has been determined and used to estimate the radial dissipation of damage energy from the radial distribution of displacements for each ion. The radial distributions of damage energy (eV/atom) are shown in Fig. 7c and 7d. The ionization energy deposited by an incident ion of specific energy to the target electrons along an incremental ion pathlength is given by the electronic stopping power (energy deposition per unit pathlength), which creates a high density of hot electrons that dissipate their energy to the atomic structure via electron-phonon coupling, leading to a highly-localized thermal transient along the ion pathlength that is generally referred to as the inelastic thermal spike, which has a duration of tens of ps to several

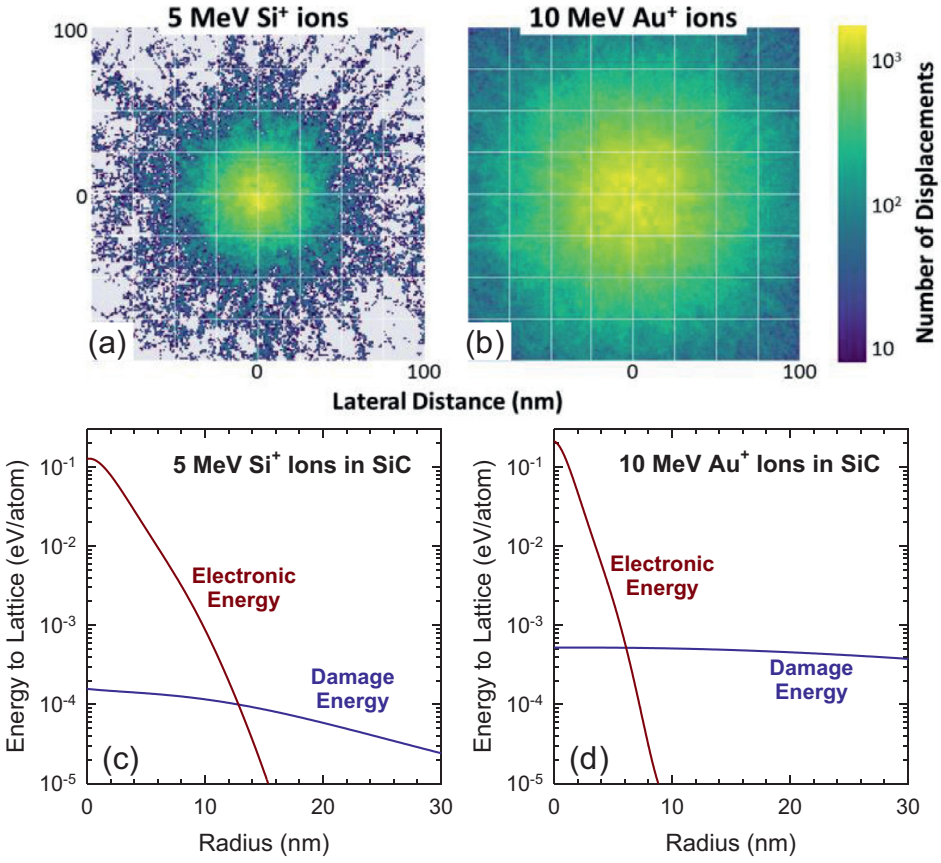

Fig. 7. Radial distribution of displacement collisions by full-cascade SRIM simulations along a segment of pathlength from 700 to 800 nm predicted for (a) 5 MeV Si ions and (b) 10 MeV Au ions. Electronic (ionization) and damage energy deposited to the atomic lattice over a pathlength of 700 to 800 nm by (c) 5 MeV Si ions and (d) 10 MeV Au ions.

hundred ps. The radial profile of electronic energy dissipation density to the lattice by 5 MeV Si and 10 MeV Au ions in SiC over the segment of pathlength from 700 to 800 nm has been calculated based on the two-temperature model and model parameters described previously for SiC [30]. The results are included in Fig. 7c and 7d. The coupling (i.e., overlap) of electronic energy and damage energy along the ion pathlength occurs over a much larger radius and with a much higher ratio of electronic to damage energy for the 5 MeV Si ions as compared to the 10 MeV Au ions, which can result in decreased defect survival along the ion trajectory for the Si ions.

The results in Fig. 3 clearly demonstrate that Au ions provide a harder primary recoil spectrum that more closely represents the primary recoil spectrum for fast neutrons in SiC compared to Si self-ions, and the results in Figs. 2, 6 and 7 suggest that defect production for Au ions is substantially higher per ion and less affected by the ionization-induced thermal spike in SiC than for Si self-ions. Using Si self-ions to achieve high doses requires at least 20 times more ion fluence than Au ions for equivalent damage depths, which leads to high concentrations of implanted Si interstitials that are highly mobile in SiC and can significantly affect microstructure evolution. On the other hand, implanted Au interstitial concentrations are significantly lower for equivalent damage doses, and Au interstitials are inert and immobile.

Conclusions

Ionization-induced annealing can have significant impacts on damage processes in irradiated materials. Complete understanding of this effect, both separately and coupled with damage energy dissipation is necessary to develop predictive models of SiC-based structural materials and electronic devices exposed to harsh radiation environments, as well as to design and interpret ion-irradiation experiments that are intended to emulate high-dose neutron damage. In this study, disorder accumulation in 3C-SiC was studied with 10 MeV Au ions and compared with previous 5 MeV Si ion data.

There is stronger coupling between inelastic and elastic process for 5 MeV Si ions, so irradiation-induced defect concentrations from the Si ions are more sensitive to dissipation of ionization energy compared to 10 MeV Au ions, where the more energetic recoil spectrum leads to weaker spatial coupling between energy dissipation processes. Consequently, resulting damage at similar dpa doses is greater from the Au ions compared to the Si ions, and Au ions have a harder recoil spectrum, more comparable to neutrons. Further, SRIM and IM3D based models of radial distributions of collision cascades, recoil spectra, energy partitioning, and displacements as a function of depths were determined. The IM3D code better predicts the Au displacements concentration as a function of depth due to its utilization of better, experimentally derived, electronic energy loss values for Au ions in SiC.

Declaration of Competing Interest

The authors declare that they have no known competing financial interests or personal relationships that could have appeared to influence the work reported in this paper.

Acknowledgments

This work was supported primarily by the Governor's Chair Program at the University of Tennessee. The irradiations and two temperature model calculations were supported by the U.S. Department of Energy, Office of Science, Basic Energy Sciences, Materials Sciences and Engineering Division under contract number DE-AC05–00OR22725. The authors are grateful to C. Ostrouchov for pysrim calculation on radial distributions of displacements. JL and YY acknowledge support for IM3D simulations from the U.S. Department of Energy, Office of Nuclear Energy's NEUP Program under Grant No. DE-NE0008827.

Supplementary material

Supplementary material associated with this article can be found, in the online version, at doi:10.1016/j.mtla.2021.101023.

References

[1] W.J. Choyke, G. Pensl, Physical properties of SiC, MRS Bull. 22 (1997) 25–29, doi:10.1557/S0883769400032723.

[2] T. Ishikawa, S. Kajii, K. Matsunaga, T. Hogami, Y. Kohtoku, T. Nagasawa, A tough, thermally conductive silicon carbide composite with high strength up to 1600°C in air, Science 282 (1998) 1295–1297, doi:10.1126/science.282.5392.1295.

[3] J.B. Wachtman, D.G. Lam, Young's modulus of various refractory materials as a function of temperature, J. Am. Ceram. Soc. 42 (1959) 254–260, doi:10.1111/j.1151-2916.1959.tb15462.x.

[4] L.L. Snead, T. Nozawa, Y. Katoh, T.S. Byun, S. Kondo, D.A. Petti, Handbook of SiC properties for fuel performance modeling, J. Nucl. Mater. 371 (2007) 329–377, doi:10.1016/j.jnucmat.2007.05.016.

[5] H. Hanchen, N. Ghoniem, Neutron displacement damage cross sections for SiC, J. Nucl. Mater. 199 (1993) 221–230, doi:10.1016/0022-3115(93)90143-M.

[6] Z. Huang, G. Liu, X. Liu, Z. Chen, D. Jiang, Manufacture of large-scale lightweight SiC mirror for space, in: Proceedings of the International Workshop on Image Processing and Optical Engineering, 2012, doi:10.1117/12.917585.

[7] P. Godignon, X. Jorda, M. Vellvehi, X. Perpina, V. Banu, D. Lopez, J. Barbero, P. Brosselard, S. Massetti, SiC Schottky diodes for harsh environment space applications, IEEE Trans. Ind. Electron. 58 (2011) 2582–2589, doi:10.1109/TIE.2010.2080252.

[8] P. Li, L. Zeng, X. Li, L. Luo, H. Zhang, M. Bo, Y. Sun, Q. Yu, M. Tang, W. Xu, B. Zhang, Analysis of the influence of single event effects on the characteristics for SiC power MOSFETs, in: Proceedings of the Prognostics and System Health Management Conference PHM-Harbin 2017, 2017, pp. 7–10, doi:10.1109/PHM.2017.8079302.

[9] P. Godignon, S. Massetti, X. Jordà, V. Soler, J. Moreno, D. Lopez, E. Maset, SiC power switches evaluation for space applications requirements, Mater. Sci. Forum 858 (2016) 852–855, doi:10.4028/www.scientific.net/MSF.858.852.

[10] R. Scheidegger, W. Santiago, K.E. Bozak, L.R. Pinero, A. Birchenough, (Invited) High power SiC power processing unit development, ECS Trans. 69 (2015) 13–19, doi:10.1149/06911.0013ecst.

[11] Y. Katoh, N. Hashimoto, S. Kondo, L.L. Snead, A. Kohyama, Microstructural development in cubic silicon carbide during irradiation at elevated temperatures, J. Nucl. Mater. 351 (2006) 228–240, doi:10.1016/j.jnucmat.2006.02.007.

[12] Y. Katoh, L.L. Snead, I. Szlufarska, W.J. Weber, Radiation effects in SiC for nuclear structural applications, Curr. Opin. Solid State Mater. Sci. 16 (2012) 143–152, doi:10.1016/j.cossms.2012.03.005.

[13] L.L. Snead, T. Nozawa, M. Ferraris, Y. Katoh, R. Shinavski, M. Sawan, Silicon carbide composites as fusion power reactor structural materials, J. Nucl. Mater. 417 (2011) 330–339, doi:10.1016/j.jnucmat.2011.03.005.

[14] R.H. Jones, L. Giancarli, A. Hasegawa, Y. Katoh, A. Kohyama, B. Riccardi, L.L. Snead, W.J. Weber, Promise and challenges of SiC_f/SiC composites for fusion energy applications, J. Nucl. Mater. 307–311 (2002) 1057–1072, doi:10.1016/S0022-3115(02)00976-5.

[15] G.S. Was, Z. Jiao, E. Getto, K. Sun, A.M. Monterrosa, S.A. Maloy, O. Anderoglu, B.H. Sencer, M. Hackett, Emulation of reactor irradiation damage using ion beams, Scr. Mater. 88 (2014) 33–36, doi:10.1016/j.scriptamat.2014.06.003.

[16] S.J. Zinkle, L.L. Snead, Opportunities and limitations for ion beams in radiation effects studies: bridging critical gaps between charged particle and neutron irradiations, Scr. Mater. 143 (2018) 154–160, doi:10.1016/j.scriptamat.2017.06.041.

[17] N. Galy, N. Toulhoat, N. Moncoffre, Y. Pipon, N. Bérerd, M.R. Ammar, P. Simon, D. Deldicque, P. Sainsot, Ion irradiation to simulate neutron irradiation in model graphites: consequences for nuclear graphite, Nucl. Instrum. Methods Phys. Res. Sect. B Beam Interact. Mater. Atoms 409 (2017) 235–240, doi:10.1016/j.nimb.2017.05.056.

[18] G.S. Was, Challenges to the use of ion irradiation for emulating reactor irradiation, J. Mater. Res. 30 (2015) 1158–1182, doi:10.1557/jmr.2015.73.

[19] S. Klaumünzer, Ion tracks in quartz and vitreous silica, Nucl. Instrum. Methods Phys. Res. Sect. B Beam Interact. Mater. Atoms 225 (2004) 136–153, doi:10.1016/j.nimb.2004.05.014.

[20] P. Kluth, C.S. Schnohr, O.H. Pakarinen, F. Djurabekova, D.J. Sprouster, R. Giulian, M.C. Ridgway, A.P. Byrne, C. Trautmann, D.J. Cookson, K. Nordlund, M. Toulemonde, Fine structure in swift heavy ion tracks in amorphous SiO_2, Phys. Rev. Lett. 101 (2008) 175503, doi:10.1103/PhysRevLett.101.175503.

[21] N. Itoh, D.M. Duffy, S. Khakshouri, A.M. Stoneham, Making tracks: electronic excitation roles in forming swift heavy ion tracks, J. Phys. Condens. Matter. 21 (2009) 474205, doi:10.1088/0953-8984/21/47/474205.

[22] E. Zarkadoula, M. Toulemonde, W.J. Weber, Additive effects of electronic and nuclear energy losses in irradiation-induced amorphization of zircon, Appl. Phys. Lett. 107 (2015) 261902, doi:10.1063/1.4939110.

[23] M. Toulemonde, W.J. Weber, G. Li, V. Shutthanandan, P. Kluth, T. Yang, Y. Wang, Y. Zhang, Synergy of nuclear and electronic energy losses in ion-irradiation processes: the case of vitreous silicon dioxide, Phys. Rev. B Condens. Matter Mater. Phys. 83 (2011) 054106, doi:10.1103/PhysRevB.83.054106.

[24] E. Zarkadoula, K. Jin, Y. Zhang, W.J. Weber, Synergistic effects of nuclear and electronic energy loss in $KTaO_3$ under ion irradiation, AIP Adv. 7 (2017) 015016, doi:10.1063/1.4973938.

[25] P. Liu, Y. Zhang, H. Xue, K. Jin, M.L. Crespillo, X. Wang, W.J. Weber, A coupled effect of nuclear and electronic energy loss on ion irradiation damage in lithium niobate, Acta Mater. 105 (2016) 429–437, doi:10.1016/j.actamat.2015.12.048.

[26] L. Thomé, A. Debelle, F. Garrido, P. Trocellier, Y. Serruys, G. Velisa, S. Miro, Combined effects of nuclear and electronic energy losses in solids irradiated with a dual-ion beam, Appl. Phys. Lett. 102 (2013) 141906, doi:10.1063/1.4801518.

[27] Y. Zhang, R. Sachan, O.H. Pakarinen, M.F. Chisholm, P. Liu, H. Xue, W.J. Weber, Ionization-induced annealing of pre-existing defects in silicon carbide, Nat. Commun. 6 (2015) 8049, doi:10.1038/ncomms9049.

[28] H. Xue, Y. Zhang, W.J. Weber, In-cascade ionization effects on defect production in 3C silicon carbide*, Mater. Res. Lett. 5 (2017) 494–500, doi:10.1080/21663831.2017.1334241.

[29] L. Nuckols, M.L. Crespillo, C. Xu, E. Zarkadoula, Y. Zhang, W.J. Weber, Coupled effects of electronic and nuclear energy deposition on damage accumulation in ion-irradiated SiC, Acta Mater. 199 (2020) 96–106, doi:10.1016/j.actamat.2020.08.014.

[30] Y. Zhang, H. Xue, E. Zarkadoula, R. Sachan, C. Ostrouchov, P. Liu, X. lin Wang, S. Zhang, T.S. Wang, W.J. Weber, Coupled electronic and atomic effects on defect evolution in silicon carbide under ion irradiation, Curr. Opin. Solid State Mater. Sci. 21 (2017) 285–298, doi:10.1016/j.cossms.2017.09.003.

[31] J.F. Ziegler, M.D. Ziegler, J.P. Biersack, SRIM - The stopping and range of ions in matter (2010), Nucl. Instrum. Methods Phys. Res. Sect. B Beam Interact. Mater. Atoms 268 (2010) 1818–1823, doi:10.1016/j.nimb.2010.02.091.

[32] C. Borschel, C. Ronning, Ion beam irradiation of nanostructures - A 3D Monte Carlo simulation code, Nucl. Instrum. Methods Phys. Res. Sect. B Beam Interact. Mater. Atoms 269 (2011) 2133–2138, doi:10.1016/j.nimb.2011.07.004.

[33] Y.G. Li, Y. Yang, M.P. Short, Z.J. Ding, Z. Zeng, J. Li, IM3D: a parallel Monte Carlo code for efficient simulations of primary radiation displacements and damage in 3D geometry, Sci. Rep. 5 (2015) 18130, doi:10.1038/srep18130.

[34] J. Li, Y. Yang, M.P. Short, More efficient and accurate simulations of primary radiation damage in materials with nanosized microstructural features or ion beams, Handbook of Materials Modeling (2020) 2381–2412, doi:10.1007/978-3-319-44680-6_115.

[35] M. Toulemonde, C. Dufour, A. Meftah, E. Paumier, Transient thermal processes in heavy ion irradiation of crystalline inorganic insulators, Nucl. Instrum. Methods Phys. Res. Sect. B Beam Interact. Mater. Atoms 166–167 (2000) 903–912, doi:10.1016/S0168-583X(99)00799-5.

[36] Y. Zhang, M.L. Crespillo, H. Xue, K. Jin, C.H. Chen, C.L. Fontana, J.T. Graham, W.J. Weber, New ion beam materials laboratory for materials modification and irradiation effects research, Nucl. Instrum. Methods Phys. Res. Sect. B Beam Interact. Mater. Atoms 338 (2014) 19–30, doi:10.1016/j.nimb.2014.07.028.

[37] W.J. Weber, Y. Zhang, Predicting damage production in monoatomic and multielemental targets using stopping and range of ions in matter code: challenges and recommendations, Curr. Opin. Solid State Mater. Sci. 23 (2019) 100757, doi:10.1016/j.cossms.2019.06.001.

[38] K. Jin, Y. Zhang, Z. Zhu, D.A. Grove, H. Xue, J. Xue, W.J. Weber, Electronic stopping powers for heavy ions in SiC and SiO_2, J. Appl. Phys. 115 (2014) 044903, doi:10.1063/1.4861642.

[39] R. Devanathan, W.J. Weber, F. Gao, Atomic scale simulation of defect production in irradiated 3C-SiC, J. Appl. Phys. 90 (2001) 2303–2309, doi:10.1063/1.1389523.

[40] A. Heft, E. Wendler, T. Bachmann, E. Glaser, W. Wesch, Defect production and annealing in ion implanted silicon carbide, Mater. Sci. Eng. B29 (1995) 142–146, doi:10.1016/0921-5107(94)04025-Y.

[41] R.E. Stoller, M.B. Toloczko, G.S. Was, A.G. Certain, S. Dwaraknath, F.A. Garner, On the use of SRIM for computing radiation damage exposure, Nucl. Instrum. Methods Phys. Res. Sect. B Beam Interact. Mater. Atoms 310 (2013) 75–80, doi:10.1016/j.nimb.2013.05.008.

[42] C. Ostrouchov, Y. Zhang, W.J. Weber, Pysrim: automation, analysis, and plotting of SRIM calculations, J. Open Source Softw. 3 (2018), doi:10.21105/joss.00829.

[43] R.S. Averback, Atomic displacement processes in irradiated metals, J. Nucl. Mater. 216 (1994) 49–62, doi:10.1016/0022-3115(94)90006-X.

[44] D. Guo, H. Zang, P. Zhang, J. Xi, T. Li, L. Ma, C. He, Analysis of primary damage in silicon carbide under fusion and fission neutron spectra, J. Nucl. Mater. 455 (2014) 229–233, doi:10.1016/j.jnucmat.2014.06.001.

[45] W.J. Weber, W. Jiang, F. Gao, R. Devanathan, Ion – solid interactions and defects in silicon carbide, Nucl. Inst. Methods Phys. Res. B 190 (2002) 261–265, doi:10.1016/S0168-583X(01)01193-4.

[46] W.J. Weber, F. Gao, R. Devanathan, W. Jiang, The efficiency of damage production in silicon carbide, Nucl. Instrum. Methods Phys. Res. Sect. B Beam Interact. Mater. Atoms 218 (2004) 68–73, doi:10.1016/j.nimb.2003.12.006.

[47] W. Jiang, Y. Zhang, W.J. Weber, Temperature dependence of disorder accumulation and amorphization in Au-ion-irradiated 6H-SiC [48, Phys. Rev. B 70 (2004) 165208, doi:10.1103/PhysRevB.70.165208.

[48] F. Gao, W.J. Weber, W. Jiang, Primary damage states produced by Si and Au recoils in SiC: a molecular dynamics and experimental investigation, Phys. Rev. B - Condens. Matter Mater. Phys. 63 (2001) 214106, doi:10.1103/PhysRevB.63.214106.

[49] W.J. Weber, L. Wang, Y. Zhang, W. Jiang, I.T. Bae, Effects of dynamic recovery on amorphization kinetics in 6H-SiC, Nucl. Instrum. Methods Phys. Res. Sect. B Beam Interact. Mater. Atoms 266 (2008) 2793–2796, doi:10.1016/j.nimb.2008.03.119.

[50] W.J. Weber, Y. Zhang, L. Wang, Review of dynamic recovery effects on ion irradiation damage in ionic-covalent materials, Nucl. Instrum. Methods Phys. Res. Sect. B Beam Interact. Mater. Atoms 277 (2012) 1–5, doi:10.1016/j.nimb.2011.12.043.